Dual-Mode Triboelectric Nanogenerator for Harvesting Water Energy and as a Self-Powered Ethanol Nanosensor

Zong-Hong Lin,[†,⊥] Gang Cheng,[†,§,⊥] Wenzhuo Wu,[†] Ken C. Pradel,[†] and Zhong Lin Wang[†,‡,*]

[†]School of Material Science and Engineering, Georgia Institute of Technology, Atlanta, Georgia 30332-0245, United States, [‡]Beijing Institute of Nanoenergy and Nanosystems, Chinese Academy of Sciences, Beijing 100083, China, and [§]Key Lab for Special Functional Materials, Henan University, Kaifeng 475004, China. [⊥]These authors contributed equally to this work.

ABSTRACT When water is passing through the air or an insulating tube, it will contain not only the mechanical energy but also the electrostatic energy due to the existence of triboelectric charges on its surface as a result of contact with the air/solid surface. In this paper, a hybrid triboelectric nanogenerator (TENG) is designed to simultaneously harvest the electrostatic and mechanical energies of flowing water. Water-TENG, mainly constructed by a superhydrophobic TiO_2 layer with hierarchical micro/nanostructures, is used to collect the electrostatic energy of water (Output 1). Contact-TENG, composed by a polytetrafluoroethylene film and a layer of assembled SiO_2 nanoparticles, is used to collect the mechanical energy of water (Output 1 and Output 2). Using TiO_2 nanomaterials in water-TENG provides the advantages of photocatalytic activity and antibacterial property for water purification. Under the impact of a water stream from a household faucet at a flowing rate of 40 mL s^{-1}, the generated short-circuit current from Output 1 and Output 2 of dual-mode TENG can reach 43 and 18 μA, respectively. The instantaneous output power densities from Output 1 and Output 2 of dual-mode TENG are 1.31 and 0.38 W m^{-2}, respectively, when connecting to a load resistor of 44 MΩ. The rectified outputs have been applied to drive light-emitting diodes and charge commercial capacitors. Besides, the water-TENG has also been demonstrated as a self-powered nanosensor for ethanol detection.

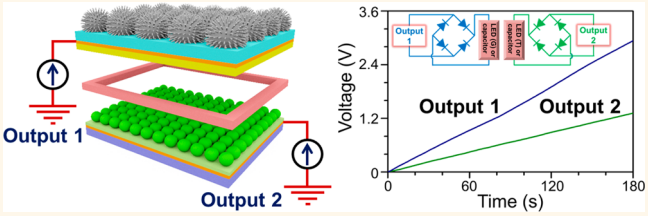

KEYWORDS: triboelectric nanogenerator · energy harvesting · self-powered nanosensor · flowing water · water drop

Self-powered nanosensors that can function without external power supply have attracted increasing attention in recent years.[1,2] For example, self-powered nanosensors toward pH,[3] temperature,[4] toxic pollutant,[5,6] light,[7,8] and biomolecule[9,10] detections have been widely researched and successfully developed. By directly harvesting energy from the environment, the self-powered nanosensors have advantages such as size minimizing and decreasing the use of environmentally unfriendly materials in batteries.[11,12] Among different energy sources, mechanical energy is the most promising candidate because it has little dependence on the daytime, weather, or even season.[13−15]

Triboelectric nanogenerator (TENG),[16] which is based on the triboelectric and electrostatic effects to harvest mechanical energy, was first invented in 2012 and has become a new energy technology.[17] As two materials in physical contact, the surface electrons/ions will transfer due to the materials with different triboelectric polarity. Then the serial separation and contact of these two materials establish electric potential differences, which will drive the electron flow through the external load and generate continuous outputs. Three fundamental operation modes of TENG, namely, vertical contact separation,[16,18] in-plane sliding,[19,20] and single electrode,[21,22] have been demonstrated and show their potential applications. Furthermore, through the modification of the materials' surfaces, the performance of TENG can be enhanced[23] and the applications are expanded to self-powered nanosensors for selective detection of metal ions[24] and small molecules.[25]

Until now, TENG has been mostly designed to operate between two solid materials and the maximum output is generated under dry conditions.[26] However, previous studies have shown that when water drops are falling from the sky or water is flowing through an insulating tube, triboelectricity will be created and cause the surface of the

* Address correspondence to zlwang@gatech.edu.

Received for review April 9, 2014 and accepted April 29, 2014.

Published online May 01, 2014
10.1021/nn501983s

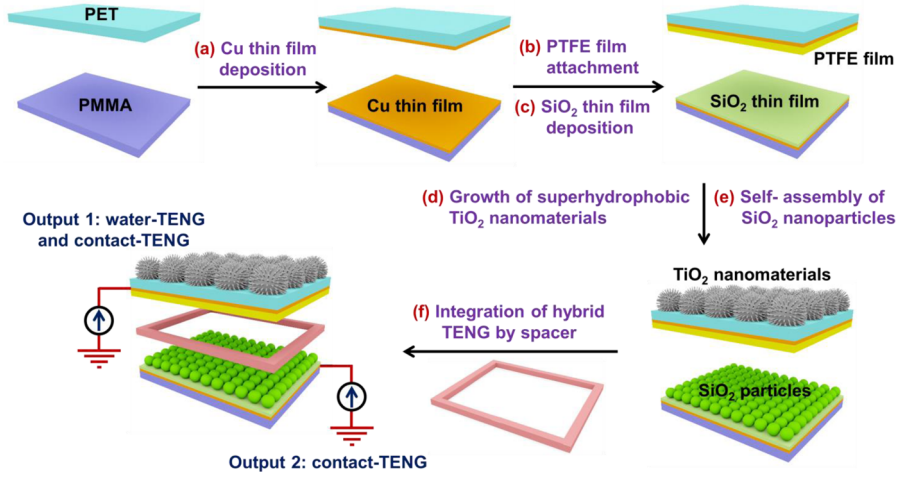

Figure 1. Fabrication process of the dual-mode TENG. (a) Cu thin films were deposited on a PET film and a PMMA sheet. (b) Commercial PTFE film was attached on the top of Cu thin film/PET film. (c) SiO_2 thin film was deposited on the top of Cu thin film/PMMA sheet. (d) TiO_2 layer with hierarchical micro/nanostructures was designed to grow on the back side of PET film. Then, the TiO_2 layer was further coated with PFTS to become a superhydrophobic surface. (e) Layer of SiO_2 nanoparticles was assembled on the deposited SiO_2 thin film in order to increase the contact area. (f) PET film was used as spacer to maintain the gap distance between the PTFE film and SiO_2 nanoparticles and combined all the parts into an integrated device. Finally, the electricity generated from water-TENG and contact-TENG can be collected through the Output 1 and Output 2 of the dual-mode TENG.

water to be positively or negatively charged.[27−30] The contact electrification between solid/water or air/water will be useful for the design of TENG. For example, we have utilized a polydimethylsiloxane (PDMS)-patterned pyramid arrays and difference sources of water (deionized, tap, and salt water) to construct TENG.[31] The developed TENG has been demonstrated with the capability to either collect the energy of water waves or act as temperature and chemical sensors. Recently, another type of TENG was proposed to collect the electrostatic energy of water drops.[32] When the charged water drops, such as rain, contact and leave the superhydrophobic polytetrafluoroethylene (PTFE) film, the electric potential differences are established and will drive the electron flow between the back metal electrode and the ground. These results are important because they discover new approaches for TENG to harvest water-related energies, which are unlimited and could be good alternatives to solar energy if we can use it for ocean waves.[30−34]

In this paper, we design a fully integrated TENG containing a water-TENG unit to collect the electrostatic energy of water and a contact-TENG unit to collect the mechanical/kinetic energy of water. Both the water-TENG and contact-TENG were operated in single-electrode mode, which already shows its convenience when harvesting energy from a continuously moving or flying object.[21,22] For the water-TENG, a superhydrophobic surface is needed in order to enhance the electrostatic induction effect.[30,32] Hence, we prepared a superhydrophobic TiO_2 layer with hierarchical micro/nanostructures to construct the water-TENG. Using TiO_2 nanomaterials can provide the water-TENG with additional functions of photocatalytic activity and antibacterial properties. An extremely positive triboelectric charging material of SiO_2 nanoparticles and an extremely negative triboelectric charging material of PTFE film were selected to build the contact-TENG. The measured signal of Output 1 of a dual-mode TENG contains the power generated from both the water-TENG and contact-TENG, while the measured signal of Output 2 of the dual-mode TENG is the power from the contact-TENG. Upon the impact of the water stream from a household faucet at a flowing rate of 40 mL/s, the generated short-circuit currents (I_{sc}) from the contact-TENG and water-TENG can reach 43 and 18 μA, respectively. The instantaneous output power density from Output 1 and Output 2 of the dual-mode TENG are 1.31 and 0.38 W m^{-2}, respectively, when connecting to a load resistor of 44 MΩ. The rectified outputs have been applied to drive light-emitting diodes (LED) and charge commercial capacitors. Alternatively, because the presence of ethanol would reduce the triboelectric charges on the water drop and decrease the electrical output, the water-TENG has been demonstrated as a self-powered nanosensor for ethanol detection. We also showed the potential that the sensing system could be simplified by replacing the electrometer with a LED.

RESULTS AND DISCUSSION

The dual-mode TENG is a fully integrated device constituted by a water-TENG and a contact-TENG. The fabrication process of dual-mode TENG is schematically depicted in Figure 1, which utilizes a polyethylene terephthalate (PET) film and a poly(methyl methacrylate) (PMMA) sheet. On the PET film, a Cu thin film (100 nm) is first deposited on one side as the electrodes for water-TENG and contact-TENG. This is the Output 1 of dual-mode

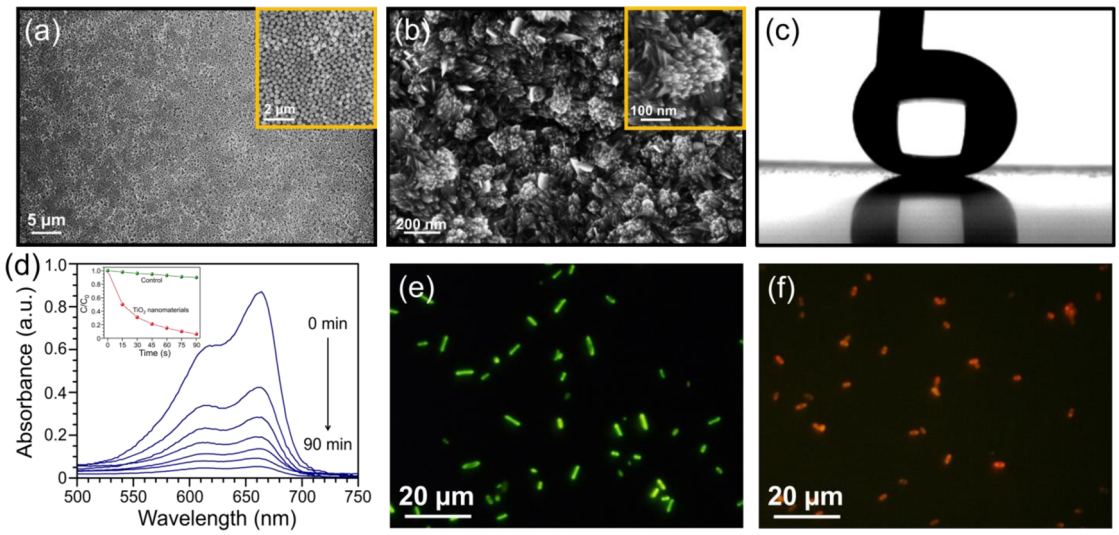

Figure 2. (a) SEM images of the assembled SiO_2 nanoparticles. Inset shows that the nanoparticles are uniformly distributed on the surface. (b) SEM images of the prepared TiO_2 layer with irregular structures. Inset shows the structures are dendrite-like particles composed by nanoplatelets. (c) Advancing contact angle of the prepared TiO_2 layer after coating with PFTS. (d) UV−vis absorption spectra of the MB solution under solar light irradiation in the presence of the prepared TiO_2 layer. The inset is the comparison of photocatalytic activity without and with the prepared TiO_2 layer. (e,f) Fluorescence images of *Escherichia coli* (*E. coli*) in LB media under solar light irradiation for 60 min without (e) and with (f) the prepared TiO_2 layer. Green and red fluorescent stains are representative of live and dead cells, respectively.

TENG, which contains the power generated from both the water-TENG and contact-TENG. Then a commercial PTFE film (25 μm) is covered on the top of the deposited Cu thin film. PTFE is purposely chosen here because it is positioned extremely negative in the triboelectric series (Figure S1, Supporting Information).[35] On the other side of the PET film, a TiO_2 layer with hierarchical micro/nanostructures is designed to grow directly through a facile, scalable, and low-cost chemical bath method. During the growth of the TiO_2 crystal, Ti(III) species are gradually oxidized to Ti(IV) species by the dissolved O_2 and then hydrolyzed to form TiO_2.[36,37] By increasing the reaction time and growth cycle, a TiO_2 layer with hierarchical micro/nanostructures instead of vertically aligned TiO_2 nanoplatelet arrays is prepared. After that, the TiO_2 layer is further coated with 1*H*,1*H*,2*H*,2*H*-perfluorooctyltrichlorosilane (PFTS) to increase the hydrophobicity. On the PMMA sheet, another Cu thin film (100 nm) is deposited on one side as the electrode of contact-TENG. This is the Output 2 of the dual-mode TENG, which is the power generated from the contact-TENG only. Therefore, the power generated by the water-TENG is the difference between Output 1 and Output 2. For the purpose of generating triboelectric charges with a high density on the surface, silica (SiO_2) is selected because it is positioned extremely positive in the triboelectric series. A SiO_2 thin film (20 nm) is deposited on the top of Cu thin film. Then a layer of SiO_2 nanoparticles is assembled on the deposited SiO_2 thin film.[38] SiO_2 nanoparticles with an average size of 250 nm are synthesized according to the Stöber method.[39] The purpose of using SiO_2 nanoparticles here is that it can provide the advantage of larger contact surface area and enhance the electric output of the contact-TENG.[24,40,41] Finally, the spacer (PET film, 0.5 mm) is applied to maintain a gap distance between the PTFE film and SiO_2 nanoparticles for the operation of the contact-TENG and combine all the parts into an integrated device.

Figure 2a displays an SEM image of assembled SiO_2 nanoparticles on the SiO_2 thin film, showing a uniform distribution of nanoparticles on the surface. Compared to that, the prepared TiO_2 layer on the PET film shows irregular structures (Figure 2b). The inset of Figure 2b further reveals that the structures are dendrite-like particles with an average size of 180 nm and composed by nanoplatelets with an average width of 5 nm and length of 70 nm. The crystal phase of the TiO_2 layer is identified by Raman spectroscopy (Figure S2a, Supporting Information) and X-ray diffraction (XRD) (Figure S2b, Supporting Information). The Raman bands appearing at 137, 254, 430, and 605 cm^{-1} can be assigned to the B_{1g}, two-phonon scattering, E_g, and A_{1g} modes of rutile phase, indicating that the dendrite-like particles are formed by rutile TiO_2 nanoplatelets.[42,43] The XRD pattern shows the characteristic diffraction peaks of rutile phase, which also validates the Raman spectroscopy result. The prepared TiO_2 layer with hierarchical micro/nanostructures in this study is of great interest not only unique in the structural features but also remarkable in the increasing of hydrophobicity.[44] In the last study,[32] we discovered that the output of water-TENG is highly related to the hydrophobicity of polymer film. This is because it will affect the contact and separation conditions between charged water drops or flowing water and the polymer film. We will discuss the working mechanism

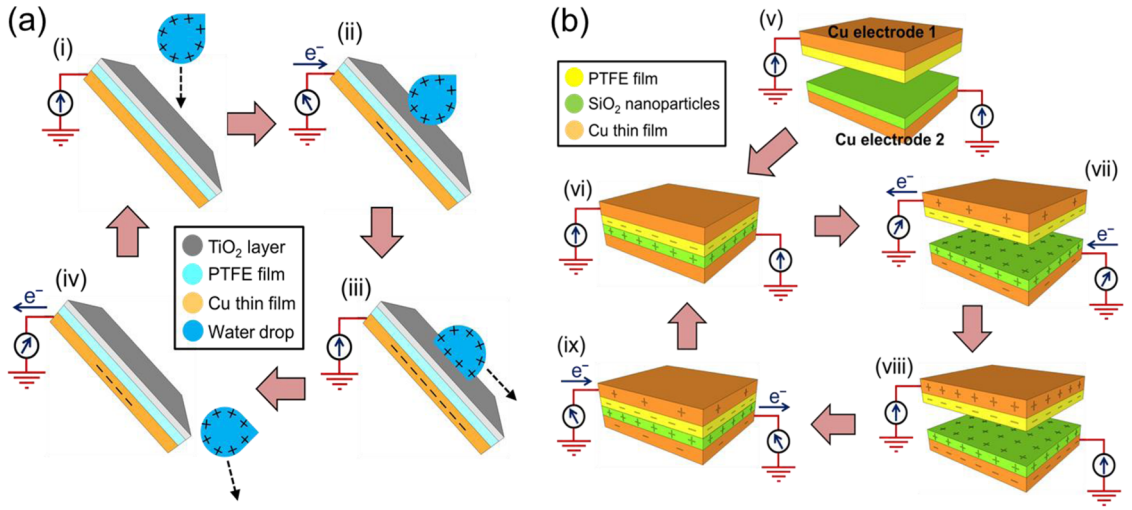

Figure 3. Working mechanisms of (a) water-TENG and (b) contact-TENG. When a charged water drop contacts the TiO_2 layer (ii), a positive electric potential difference will be formed and causes the electrons to flow from the ground to the Cu electrode, finally reaching equilibrium (iii). Once the charged water drop leaves the TiO_2 layer, a negative electric potential difference will be formed and forces the electrons to flow from the Cu electrode to the ground (iv), until achieving another equilibrium (i). Alternatively, the impact force from the water drop also makes the PTFE film contact the SiO_2 nanoparticles, causing the SiO_2 nanoparticle and PTFE film charged surfaces (vi). As the water drop leaves, the contacted surfaces are separated, then a positive electric potential difference between the SiO_2 nanoparticles and the ground and a negative electric potential difference between the ground and the PTFE film will be established (vii). This causes the electrons to flow from the ground to the Cu electrode 2 and from the Cu electrode 1 to the ground, finally reaching equilibrium (viii). Once another water drop falls, a negative electric potential difference between the SiO_2 nanoparticles and the ground and a positive electric potential difference between the ground and the PTFE film will be formed. This forces the electrons to flow from the Cu electrode 2 to the ground and from the ground to the Cu electrode 1 (ix), until achieving another equilibrium (vi).

of water-TENG in more detail later. The hydrophobicity of TiO_2 layer is investigated by measuring the contact angle of water drops. The measured contact angle of the TiO_2 layer is around 130° (Figure S3, Supporting Information). Compared to the rutile form of the smooth TiO_2 surface with a contact angle less than 80°,[45] the increase of contact angle of the TiO_2 layer is because the hierarchical micro/nanostructures will contain trapped air, which then reduce the actual contact area between the surface and water drops. With a monolayer coating of PFTS on the TiO_2 layer, the measured contact angle of TiO_2 layer can be enhanced to 156°, which can be defined as a superhydrophobic surface (Figure 2c).

Different from our previous study using a superhydrophobic PTFE film to fabricate the water-TENG,[32] we vary the composition of PTFE to TiO_2 and fabricate a new type of water-TENG in this paper. TiO_2 is selected due to its low cost, high chemical stability, excellent photocatalytic activity, and broad-spectrum antibacterial property.[46,47] All of these characteristics indicate that the water-TENG composed by TiO_2 can not only harvest the electrostatic energy of water but also provide additional function of purifying water. The photocatalytic activity of the TiO_2 layer was evaluated by the photodegradation of methylene blue (MB) under solar light irradiation (intensity 100 mW cm^{-2}) (Figure 2d). In a typical experiment, the TiO_2 layer on the PET film was dipped into a MB solution (10 mL, 20 μM) and kept in the dark for 20 min to reach an adsorption−desorption equilibrium between the TiO_2 layer and MB before light irradiation. After the light irradiation for 90 min, we can observe that almost all MB is photodegradated as compared to the control experiment in the absence of the TiO_2 layer. The antibacterial property of the TiO_2 layer against *E. coli* was also assessed. Representative microscopic images of *E. coli* in LB media incubating without and with the TiO_2 layer under light irradiation for 30 min are displayed in Figure 2e and 2f. The green and red objects correspond to live and dead *E. coli*, respectively. The viability values of *E. coli* in the presence of the TiO_2 layer without and with light irradiation are 84 and 17%, respectively.

The working mechanism of dual-mode TENG can be illustrated separately as a water-TENG (Figure 3a) and a contact-TENG (Figure 3b). Both the water-TENG and contact-TENG are operated in single-electrode mode.[21,22] For example, when a water drop carrying positive charges contacts the TiO_2 layer (ii), a positive electric potential difference will be formed between the charged water drop and the ground. This causes the electrons to flow from the ground to the Cu electrode and generate an instantaneously opposite potential to balance the electric field, finally reaching equilibrium (iii). Once the charged water drop leaves the TiO_2 layer, a negative electric potential difference will be formed, forcing the electrons to flow from the Cu electrode to the ground (iv), until

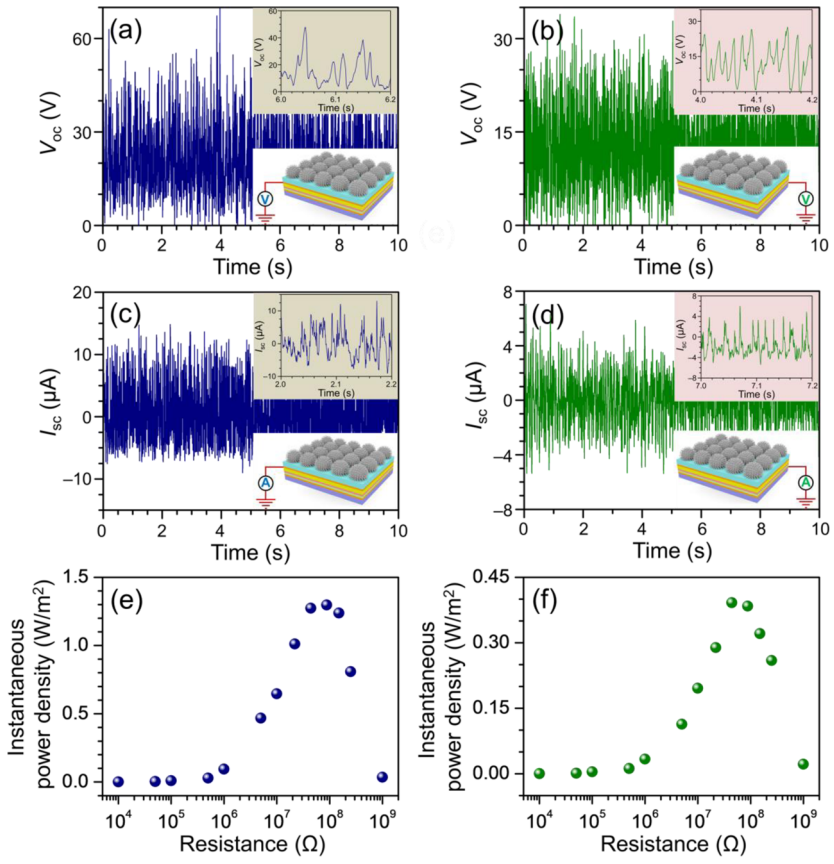

Figure 4. (a,b) Generated V_{oc} from Output 1 (a) and Output 2 (b) of dual-mode TENG under the impact of the flowing water from a household faucet. (c,d) Generated I_{sc} from Output 1 (c) and Output 2 (d) of dual-mode TENG under the impact of the flowing water from a household faucet. The flowing rate of water was set up at 20 mL s^{-1}, and the distance between the dual-mode TENG and the outlet of the faucet was 25 cm. (e,f) Dependence of instantaneous power density from Output 1 (e) and Output 2 (f) of dual-mode TENG on the resistance of the external load. The effective dimensions of dual-mode TENG demonstrated here are 1.2 cm × 1.2 cm.

achieving another equilibrium (i). The triboelectricity generated during the contact electrification process with the TiO_2 layer surface could also contribute to the output of the water-TENG.[32] However, in our study, this contribution would be minor because the triboelectric charges are largely generated when water is flowing through the pipe.[27−30]

Alternatively, the impact force from the water drop also drives the contact-TENG to work. The impact force will make the PTFE film contact the SiO_2 nanoparticles (vi), causing the electron transfer from the SiO_2 nanoparticles to the PTFE film surface and leaving the SiO_2 nanoparticles on a positively charged surface.[42] As the water drop leaves the dual-mode TENG (the TiO_2 layer), the contacted surfaces are separated, then a positive electric potential difference between the SiO_2 nanoparticles and the ground and a negative electric potential difference between the ground and the PTFE film will be established (vii). This causes the electrons to flow from the ground to the Cu electrode 2 and from the Cu electrode 1 to the ground, finally reaching equilibrium (viii). This contributes to instantaneously positive and negative currents from the Output 2 and Output 1 of dual-mode TENG. Once another charged water drop falls on the dual-mode TENG and makes the PTFE film contact the SiO_2 nanoparticles again, a negative electric potential difference between the SiO_2 nanoparticles and the ground and a positive electric potential difference between the ground and the PTFE film will be formed. This causes the electrons to flow from the Cu electrode 2 to the ground and from the ground to the Cu electrode 1 (ix), until achieving another equilibrium (vi). This process corresponds to instantaneously negative and positive currents from the Output 2 and Output 1 of dual-mode TENG. So from the working mechanism of dual-mode TENG, when a charged water drop falls on the dual-mode TENG, the generated outputs of water-TENG and contact-TENG will be simultaneous and in the same direction. This is also why we design the same output (Output 1) for the water-TENG and contact-TENG. If the charged water drop or flowing water contact and leave the dual-mode TENG periodically, both the outputs of water-TENG and contact-TENG will be continuously generated.

The performance of dual-mode TENG was tested by using the flowing water from a household faucet. Here we need to explain that the output of dual-mode TENG

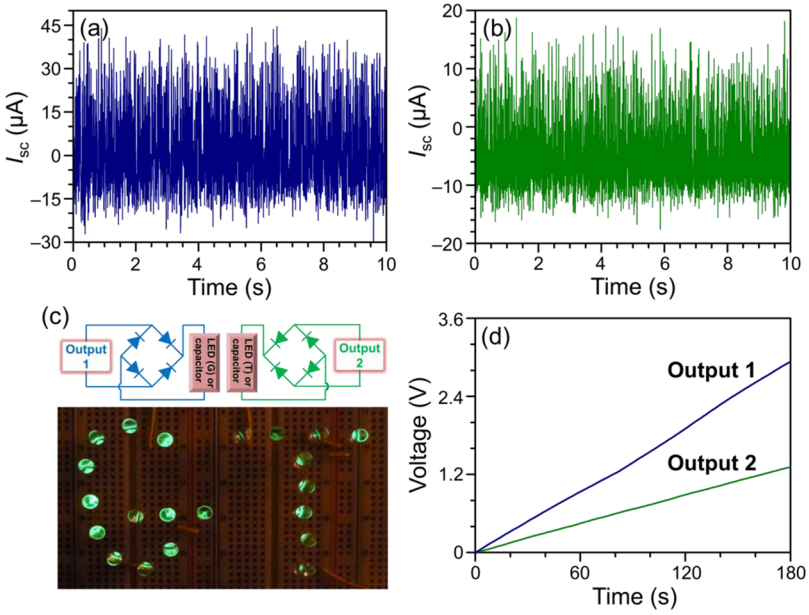

Figure 5. (a,b) Generated I_{sc} from Output 1 (a) and Output 2 (b) of dual-mode TENG under the impact of the flowing water from a household faucet. The flowing rate of water was set up at 40 mL s^{-1}, and the distance between the dual-mode TENG and the outlet of the faucet was 25 cm. (c) Diagram of corresponding circuit connection polarities and the photograph of the rectified outputs from Output 1 and Output 2 of dual-mode TENG to drive commercial LEDs. (d) Charging curves of 33 μF capacitors by the rectified outputs from Output 1 and Output 2 of dual-mode TENG. The effective dimensions of dual-mode TENG demonstrated here are 3.3 cm × 3.3 cm.

generated is based on the change of water amount on the TiO_2 layer surface. It is clear that the water flowing from the faucet is not fully continuous (video S1, Supporting Information). The water flowing from the faucet has some fluctuation and causes the amount of water on the TiO_2 layer surface to be constantly changing. Besides, the superhydrophobic property of the TiO_2 nanomaterials also enables the change of water amount on the surface. The flowing rate of water was controlled at 20 mL s^{-1}, and the distance between the dual-mode TENG and the outlet of faucet was 25 cm. The impact angle was optimized at 30°. The open-circuit voltage (V_{oc}) and I_{sc} were measured to evaluate the performance of dual-mode TENG. The typical V_{oc} and I_{sc} curves generated from Output 1 and Output 2 of dual-mode TENG are shown in Figure 4. The V_{oc} values of Output 1 (Figure 4a) and Output 2 (Figure 4b) achieve 52 and 35 V, respectively, and the I_{sc} values of Output 1 and Output 2 exceed 14 μA (Figure 4c) and 6.7 μA (Figure 4d), respectively. To investigate the output power density of dual-mode TENG, we also measured the generated voltage and current from Output 1 and Output 2 of dual-mode TENG when connected to an external load resistor. The resistance was varied from 0.01 MΩ to 1 GΩ. As the results displayed in Figure S4 show (Supporting Information), when the resistance is below 0.1 MΩ, the generated voltage from Output 1 and Output 2 of dual-mode TENG close to 0 and the generated current from Output 1 and Output 2 of dual-mode TENG have only slight changes. However, when the resistance is increased from 0.1 MΩ to 1 GΩ, the generated voltage from Output 1 and Output 2 of dual-mode TENG through the load will generally increase, but the generated current from Output 1 and Output 2 of dual-mode across the load will decrease. As a result, the instantaneous power density generated from Output 1 and Output 2 of dual-mode remains small with the resistance below 0.1 MΩ and achieves the maximum values of 1.31 and 0.38 W m^{-2} at a resistance of 44 MΩ, respectively.

To address the potential applications of the TENG, we increased the effective dimensions of dual-mode TENG to 3.3 cm × 3.3 cm (Figure S5, Supporting Information) and increased the flowing rate of water at 40 mL s^{-1}. The generated I_{sc} from Output 1 (Figure 5a) and Output 2 (Figure 5b) of dual-mode TENG can reach 43 and 18 μA, respectively. Besides, we also measured the generated I_{sc} from a single water-TENG (Figure S6, Supporting Information). The value of generated I_{sc} is 30 μA, which is smaller than the Output 1 of the dual-mode TENG. This result verifies the proposed working mechanism of dual-mode TENG in Figure 3 that the generated outputs of water-TENG and contact-TENG are simultaneous and in the same direction. By integrating the I_{sc} peak, we can deduce that collected charges from Output 1 and Output 2 of dual-mode TENG in a unit of time are 3.3 and 1.4 μQ s^{-1}, respectively. Then we applied the full-wave rectifying bridge to further transform the AC outputs to pulse outputs in the same direction. The rectified outputs from Output 1 and Output 2 of dual-mode TENG can be used to drive commercial LEDs (Figure 5c and video S1,

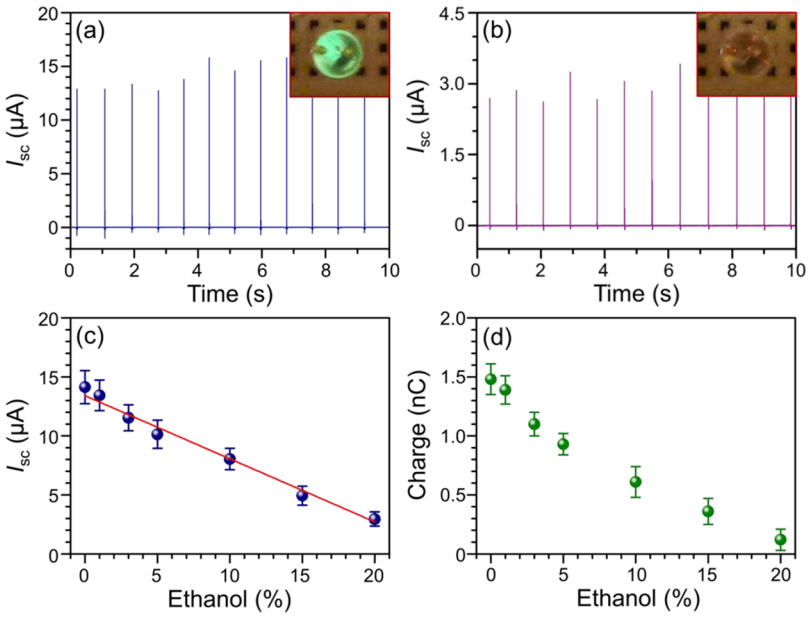

Figure 6. Water-TENG as a self-powered ethanol sensor. (a) Output I_{sc} of water-TENG generated by deionized water drops. Inset photograph shows that the generated output is capable of turning on a commercial LED as an indicator. (b) Output I_{sc} of water-TENG generated by a solution containing 20% ethanol (percentage by volume). Inset photograph shows that the generated output cannot drive the commercial LED. (c) Output I_{sc} value of water-TENG generated by samples containing different concentrations of ethanol. (d) Inductively transferred charges of water-TENG generated by samples containing different concentration of ethanol. The values are obtained by integrating the I_{sc} peaks of water-TENG generated by samples containing different concentrations of ethanol. All of the experiments were conducted using a syringe pump system to control the volume of each sample drop (30 μL), and each sample drop fell from a height of 50 cm.

Supporting Information) and charge 33 μF capacitors (Figure 5d).

Furthermore, we demonstrated another application of water-TENG to be used as a self-powered nanosensor for ethanol detection. To realize the concept, a syringe pump system was used to control the volume of each sample drop (30 μL). The sample drop was set up to fall from a height of 50 cm. Figure 6a displays the output I_{sc} of water-TENG generated by deionized water drops. The output I_{sc} reaches a value of 14 μA. However, when the sample is changed from deionized water to a solution containing 20% ethanol (percentage by volume), the generated I_{sc} of the water-TENG is decreased to 3 μA (Figure 6b). The relationship between the generated I_{sc} and ethanol concentration is shown in Figure 6c. By connecting the water-TENG to a LED (indicator), a stand-alone and self-powered ethanol nanosensor has been developed. The inset of Figure 6b reveals that the LED went out when detecting the 20% ethanol solution. The decrease of generated I_{sc} probably comes from the reduced charges on the sample drop. By integrating the I_{sc} peak of water-TENG generated at different ethanol concentration, we can deduce the inductively transferred charges on the Cu electrode, which is proportional to the triboelectric charges on the sample drop. It is clearly shown that the triboelectric charges on the sample drop are decreased when ethanol concentration is increased (Figure 6d). Previous studies have verified that ethanol has the ability to remove the triboelectric charges.[48,49] Hence, the presence of ethanol will reduce the triboelectric charges on the sample drop surface and decrease the electrical output of water-TENG. Compared to another self-powered ethanol sensor based on the contact electrification of a hydrophobic polymer film and sample,[31] the as-developed water-TENG not only is a new design but also has the advantage of minimizing the sample volume.

CONCLUSION

In summary, a dual-mode TENG constituted by a water-TENG and contact-TENG has been developed and demonstrated to harvest the electrostatic and mechanic energies of water and act as a self-powered nanosensor for ethanol detection. Upon the impact of a water stream from a household faucet, the generated I_{sc} from Output 1 and Output 2 of the dual-mode TENG achieves 43 and 18 μA, respectively. The instantaneous output power densities from Output 1 and Output 2 of the dual-mode TENG are 1.31 and 0.38 W m^{-2}, respectively, when connecting to a load resistor of 44 MΩ. The rectified outputs have been demonstrated to drive LEDs and charge commercial capacitors. All of these results show that the dual-mode TENG has the potential to effectively harvest the flowing water and water drop energies in the environment. In addition, using superhydrophobic TiO_2 layer with hierarchical micro/nanostructures in water-TENG shows the potential

applications of photocatalytic activity and antibacterial property for water purification. The combination of a commercial LED with water-TENG indicates that the sensing system toward ethanol detection could be simplified in the future by replacing the electrometer with an LED.

METHODS SUMMARY

Preparation of the Superhydrophobic TiO_2 Layer. Before the growth of the TiO_2 layer with hierarchical micro/nanostructures, the purchased PET film (0.1 mm) was ultrasonically cleaned in ethanol and water for 30 min. Then the PET film was placed in a glass bottle filled with $TiCl_3$ solution (0.1 M). After 10 min, the glass bottle was heated in an oven at 80 °C for 6 h and cooled in air. The growth cycle needed to be repeated two times to make sure the PET film surface was coated with a uniform TiO_2 layer. The TiO_2-coated PET film was rinsed with water to remove the nonadsorbed TiO_2 nanomaterials and dried at ambient temperature. Finally, the TiO_2-coated PET film was immersed in 0.5% PFTS in hexane for 10 min and washed with hexane to remove residual PFTS. After being further dried at ambient temperature, the TiO_2-coated PET film was treated in a vacuum oven at 110 °C for 1 h.

Fabrication of the Dual-Mode TENG. The fabrication process of dual-mode TENG was started from two substrates of polyethylene terephthalate film and poly(methyl methacrylate) sheet. On the PET film, the superhydrophobic TiO_2 layer had already been prepared on one side. On the other side, a Cu thin film (100 nm) was deposited as the electrodes of water-TENG and contact-TENG and the Output 1 of dual-mode TENG. Then a commercial PTFE film (25 μm) was covered on the top of deposited Cu thin film. On the PMMA sheet, another Cu thin film (100 nm) was deposited on one side as the electrode of contact-TENG and the Output 2 of dual-mode TENG. Then a SiO_2 thin film (20 nm) was deposited on the top of Cu thin film. A layer of SiO_2 nanoparticles was further assembled on the deposited SiO_2 thin film.[38] SiO_2 nanoparticles with an average size of 250 nm were synthesized according to the Stöber method.[39] Typically, concentrated ammonia (28%, 3 mL) was added rapidly to the solution containing absolute ethanol (99.9%, 50 mL) and tetraethyl orthosilicate (99%, 1.5 mL). The mixture was reacted at ambient temperature for 24 h. Finally, another PET film (0.5 mm) was used as the spacer to maintain the gap distance between the PTFE film and SiO_2 nanoparticles and combine all the parts into an integrated device.

Characterization. A Hitachi SU8010 field emission scanning electron microscope (SEM) was used to measure the size and shape of TiO_2 hierarchical micro/nanostructures and the assembled SiO_2 nanoparticles. A programmable syringe pump (PHD 2000, Harvard Apparatus) was applied to control the volume of each sample drop in the experiment of the ethanol sensor. For the measurement of electrical outputs of TENG, a programmable electrometer (Keithley model 6514) and a low-noise current preamplifier (Stanford Research System model SR570) were used. A 450 W xenon arc lamp (Oriel, Stratford, CT) equipped with an AM 1.5 filter was used as a solar irradiation source in the photocatalytic and antibacterial tests. A commercially available silicon-based reference cell was employed to examine the light intensity (100 mW cm^{-2}).

Conflict of Interest: The authors declare no competing financial interest.

Acknowledgment. This work was supported by MURI (Airforce Researcg Lab), Office of Basic Energy Sciences (DE-FG02-07ER46394), U.S. Department of Energy, NSF, NSFC (61176067), a joint project with Sungkyunkwan University, Korea, and the "thousands talents" program for pioneer researcher and his innovation team, China, Beijing City Committee of science and technology project (Z131100006013004). Patents have been filed based on the research presented here.

Supporting Information Available: More detailed information about the triboelectric series, the contact angle, Raman, and XRD data of TiO_2 layer, the dependence of output voltage and current from Output 1 and Output 2 of dual-mode TENG on the resistance of the external load, the scheme of the dual-mode TENG with dimensions of 3.3 cm × 3.3 cm, and the generated I_{sc} from a single water-TENG. This material is available free of charge *via* the Internet at http://pubs.acs.org.

REFERENCES AND NOTES

1. Wang, Z. L.; Song, J. Piezoelectric Nanogenerators Based on Zinc Oxide Nanowire Arrays. *Science* **2006**, *312*, 242–246.
2. Wang, Z. L. Self-Powered Nanosensors and Nanosystems. *Adv. Mater.* **2012**, *24*, 280–285.
3. Xu, S.; Qin, Y.; Xu, C.; Wei, Y.; Yang, R.; Wang, Z. L. Self-Powered Nanowire Devices. *Nat. Nanotechnol.* **2010**, *5*, 366–R373.
4. Yang, Y.; Lin, Z.-H.; Hou, T.; Zhang, F.; Wang, Z. L. Nanowire-Composite Based Flexible Thermoelectric Nanogenerators and Self-Powered Temperature Sensors. *Nano Res.* **2012**, *5*, 888–895.
5. Lee, M.; Bae, J.; Lee, J.; Lee, C.-S.; Hong, S.; Wang, Z. L. Self-Powered Environmental Sensor System Driven by Nanogenerators. *Energy Environ. Sci.* **2011**, *4*, 3359–3363.
6. Wen, D.; Deng, L.; Guo, S.; Dong, S. Self-Powered Sensor for Trace Hg^{2+} Detection. *Anal. Chem.* **2011**, *83*, 3968–3972.
7. Tian, B.; Zheng, X.; Kempa, T. J.; Fang, Y.; Yu, N.; Yu, G.; Huang, J.; Lieber, C. M. Coaxial Silicon Nanowires as Solar Cells and Nanoelectronic Power Sources. *Nature* **2007**, *449*, 885–889.
8. Lin, Z.-H.; Cheng, G.; Yang, Y.; Zhou, Y. S.; Lee, S.; Wang, Z. L. Triboelectric Nanogenerator as an Active UV Photodetector. *Adv. Funct. Mater.* **2014**, 10.1002/adfm.201302838.
9. Katz, E.; Bückmann, A. F.; Willner, I. Self-Powered Enzyme-Based Biosensors. *J. Am. Chem. Soc.* **2001**, *123*, 10752–10753.
10. Deng, L.; Chen, C.; Zhou, M.; Guo, S.; Wang, E.; Dong, S. Integrated Self-Powered Microchip Biosensor for Endogenous Biological Cyanide. *Anal. Chem.* **2010**, *82*, 4283–4287.
11. Wang, Z. L. Self-Powered Nanotech. *Sci. Am.* **2008**, *298*, 82–87.
12. Akyildiz, I. F.; Jornet, J. M. Electromagnetic Wireless Nanosensor Networks. *Nano Commun. Networks* **2010**, *1*, 3–19.
13. Mitcheson, P. D.; Miao, P.; Stark, B. H.; Yeatman, E. M.; Holmes, A. S.; Green, T. C. MEMS Electrostatic Micro-Power Generator for Low Frequency Operation. *Sens. Actuators, A* **2004**, *115*, 523–529.
14. Beeby, S. P.; Torah, R. N.; Tudor, M. J.; Glynne-Jones, P.; O'Donnell, T.; Saha, C. R.; Roy, S. A Micro Electromagnetic Generator for Vibration Energy Harvesting. *J. Micromech. Microeng.* **2007**, *17*, 1257–1265.
15. Naruse, Y.; Matsubara, N.; Mabuchi, K.; Izumi, M.; Suzuki, S. Electrostatic Micro Power Generation from Low-Frequency Vibration Such as Human Motion. *J. Micromech. Microeng.* **2009**, *19*, 094002.
16. Fan, F.-R.; Tian, Z.-Q.; Wang, Z. L. Flexible Triboelectric Generator. *Nano Energy* **2012**, *1*, 328–334.
17. Wang, Z. L. Triboelectric Nanogenerators as New Energy Technology for Self-Powered Systems and as Active Mechanical and Chemical Sensors. *ACS Nano* **2013**, *7*, 9533–9557.
18. Fan, F.-R.; Lin, L.; Zhu, G.; Wu, W.; Zhang, R.; Wang, Z. L. Transparent Triboelectric Nanogenerators and Self-Powered Pressure Sensors Based on Micropatterned Plastic Films. *Nano Lett.* **2012**, *12*, 3109–3114.
19. Zhu, G.; Chen, J.; Liu, Y.; Bai, P.; Zhou, Y. S.; Jing, Q. S.; Pan, C. F.; Wang, Z. L. Linear-Grating Triboelectric Generator Based on Sliding Electrification. *Nano Lett.* **2013**, *13*, 2282–2289.

20. Wang, S. H.; Lin, L.; Xie, Y.; Jing, Q. S.; Niu, S. M.; Wang, Z. L. Sliding-Triboelectric Nanogenerators Based on In-Plane Charge-Separation Mechanism. *Nano Lett.* **2013**, *13*, 2226–2233.
21. Yang, Y.; Zhou, Y. S.; Zhang, H. L.; Chen, J.; Liu, Y.; Lee, S. M.; Wang, Z. L. A Single-Electrode Based Triboelectric Nanogenerator as Self-Powered Tracking System. *Adv. Mater.* **2013**, *25*, 6594–6601.
22. Cheng, G.; Lin, Z.-H.; Du, Z.; Wang, Z. L. Increase Output Energy and Operation Frequency of a Triboelectric Nanogenerator by Two Grounded Electrodes Approach. *Adv. Funct. Mater.* **2014**, 10.1002/adfm.201303659.
23. Zhang, X.-S.; Han, M.-D.; Wang, R.-X.; Meng, B.; Zhu, F.-Y.; Sun, X.-M.; Hu, W.; Wang, W.; Li, Z.-H.; Zhang, H.-X. High-Performance Triboelectric Nanogenerator with Enhanced Energy Density Based on Single-Step Fluorocarbon Plasma Treatment. *Nano Energy* **2014**, *4*, 123–131.
24. Lin, Z.-H.; Zhu, G.; Zhou, Y. S.; Yang, Y.; Bai, P.; Chen, J.; Wang, Z. L. A Self-Powered Triboelectric Nanosensor for Mercury Ion Detection. *Angew. Chem., Int. Ed.* **2013**, *52*, 5065–5069.
25. Lin, Z.-H.; Xie, Y.; Yang, Y.; Wang, S.; Zhu, G.; Wang, Z. L. Enhanced Triboelectric Nanogenerators and Triboelectric Nanosensor Using Chemically Modified TiO_2 Nanomaterials. *ACS Nano* **2013**, *7*, 4554–4560.
26. Nguyen, V.; Yang, R. Effect of Humidity and Pressure on the Triboelectric Nanogenerator. *Nano Energy* **2013**, *2*, 604–608.
27. Takahashi, T. Measurement of Electric Charge of Cloud Droplets, Drizzle, and Raindrops. *Rev. Geophys.* **1973**, *11*, 903–924.
28. Ravelo, B.; Duval, F.; Kane, S.; Nsom, B. Demonstration of the Triboelectricity Effect by the Flow of Liquid Water in the Insulating Pipe. *J. Electrost.* **2011**, *69*, 473–478.
29. Choi, D.; Lee, H.; Im, D. J.; Kang, I. S.; Lim, G.; Kim, D. S.; Kang, K. H. Spontaneous Electrical Charging of Droplets by Conventional Pipetting. *Sci. Rep.* **2013**, *3*, 2037.
30. Cheng, G.; Lin, Z.-H.; Du, Z.-L.; Wang, Z. L. Simultaneously Harvesting Electrostatic and Mechanical Energies from Flowing Water by a Hybridized Triboelectric Nanogenerator. *ACS Nano* **2014**, *8*, 1932–1939.
31. Lin, Z.-H.; Cheng, G.; Lin, L.; Lee, S.; Wang, Z. L. Water–Solid Surface Contact Electrification and Its Use for Harvesting Liquid-Wave Energy. *Angew. Chem., Int. Ed.* **2013**, *52*, 12545–12549.
32. Lin, Z.-H.; Cheng, G.; Lee, S.; Pradel, K. C.; Wang, Z. L. Harvesting Water Drop Energy by a Sequential Contact-Electrification and Electrostatic-Induction Process. *Adv. Mater.* **2014**, DOI: adma.201400373R2 (accepted for publication).
33. Ma, M.; Guo, L.; Anderson, D. G.; Langer, R. Bio-Inspired Polymer Composite Actuator and Generator Driven by Water Gradients. *Science* **2013**, *339*, 186–189.
34. Moon, J. K.; Jeong, J.; Lee, D.; Pak, H. K. Electrical Power Generation by Mechanically Modulating Electrical Double Layers. *Nat. Commun.* **2013**, *4*, 1847.
35. McCarty, L. S.; Whitesides, G. M. Electrostatic Charging Due to Separation of Ions at Interfaces: Contact Electrification of Ionic Electrets. *Angew. Chem., Int. Ed.* **2008**, *47*, 2188–2207.
36. Hosono, E.; Fujihara, S.; Kakiuchi, K.; Imai, H. Growth of Submicrometer-Scale Rectangular Parallelepiped Rutile TiO_2 Films in Aqueous $TiCl_3$ Solutions under Hydrothermal Conditions. *J. Am. Chem. Soc.* **2004**, *126*, 7790–7791.
37. Hoang, S.; Berglund, S. P.; Fullon, R. R.; Minter, R. L.; Mullins, C. B. Chemical Bath Deposition of Vertically Aligned TiO_2 Nanoplatelet Arrays for Solar Energy Conversion Applications. *J. Mater. Chem. A* **2013**, *1*, 4307–4315.
38. Jiang, P.; Bertone, J. F.; Hwang, K. S.; Colvin, V. L. Single-Crystal Colloidal Multilayers of Controlled Thickness. *Chem. Mater.* **1999**, *11*, 2132–2140.
39. Stöber, W.; Fink, A.; Bohn, E. Controlled Growth of Monodisperse Silica Spheres in the Micron Size Range. *J. Colloid Interface Sci.* **1968**, *26*, 62–69.
40. Zhu, G.; Lin, Z.-H.; Jing, Q. S.; Bai, P.; Pan, C. F.; Yang, Y.; Zhou, Y. S.; Wang, Z. L. Toward Large-Scale Energy Harvesting by a Nanoparticle-Enhanced Triboelectric Nanogenerator. *Nano Lett.* **2013**, *13*, 847–853.
41. Cheng, G.; Lin, Z.-H.; Lin, L.; Du, Z.-L.; Wang, Z. L. Pulsed Nanogenerator with Huge Instantaneous Output Power Density. *ACS Nano* **2013**, *7*, 7383–7391.
42. Zhang, J.; Li, M.; Feng, Z.; Chen, J.; Li, C. UV Raman Spectroscopic Study on TiO_2. I. Phase Transformation at the Surface and in the Bulk. *J. Phys. Chem. B* **2006**, *110*, 927–935.
43. Mazza, T.; Barborini, E.; Piseri, P.; Milani, P. Raman Spectroscopy Characterization of TiO_2 Rutile Nanocrystals. *Phys. Rev. B* **2007**, *75*, 045416.
44. Feng, X.; Zhai, J.; Jiang, L. The Fabrication and Switchable Superhydrophobicity of TiO_2 Nanorod Films. *Angew. Chem., Int. Ed.* **2005**, *44*, 5115–5118.
45. Wang, R.; Sakai, N.; Fujishima, A.; Watanabe, T.; Hashimoto, K. Studies of Surface Wettability Conversion on TiO_2 Single-Crystal Surfaces. *J. Phys. Chem. B* **1999**, *103*, 2188–2194.
46. Chen, X.; Mao, S. S. Titanium Dioxide Nanomaterials: Synthesis, Properties, Modifications, and Applications. *Chem. Rev.* **2007**, *107*, 2891–2959.
47. Chen, F. N.; Yang, X. D.; Xu, F. F.; Wu, Q.; Zhang, Y. P. Correlation of Photocatalytic Bactericidal Effect and Organic Matter Degradation of TiO_2 Part I: Observation of Phenomena. *Environ. Sci. Technol.* **2009**, *43*, 1180–1184.
48. Burgo, T. A. L.; Ducati, T. R. D.; Francisco, K. R.; Clinckspoor, K. J.; Galembeck, F.; Galembeck, S. E. Triboelectricity: Macroscopic Charge Patterns Formed by Self-Arraying Ions on Polymer Surfaces. *Langmuir* **2012**, *28*, 7407–7416.
49. Santos, L. P.; Bernardes, J. S.; Galembeck, F. Corona-Treated Polyethylene Films Are Macroscopic Charge Bilayers. *Langmuir* **2013**, *29*, 892–901.